The high-energy radiation environment of the habitable-zone super-Earth LHS 1140b

R. Spinelli[1], F. Borsa[2], G. Ghirlanda[1,2], G. Ghisellini[2], S. Campana[2], F. Haardt[3,4], and E. Poretti[2,5]

[1] Dipartimento di Fisica G. Occhialini, Università Milano-Bicocca, Piazza della Scienza 3, 20126 Milano, Italy
e-mail: r.spinelli5@campus.unimib.it
[2] INAF – Osservatorio Astronomico di Brera, Via E. Bianchi 46, 23807 Merate (LC), Italy
[3] Dipartimento di Scienza e Alta Tecnologia, Università dell'Insubria, Via Valleggio 11, 22100 Como, Italy
[4] INFN – Sezione Milano-Bicocca, Piazza della Scienza 3, 20126 Milano, Italy
[5] Fundación Galileo Galilei – INAF, Rambla José Ana Fernandez Pérez 7, 38712 Breña Baja, TF, Spain

ABSTRACT

Context. In the last few years many exoplanets in the habitable zone (HZ) of M-dwarfs have been discovered, but the X-ray/UV activity of cool stars is very different from that of our Sun. The high-energy radiation environment influences the habitability, plays a crucial role for abiogenesis, and impacts the chemistry and evolution of planetary atmospheres. LHS 1140b is one of the most interesting exoplanets discovered. It is a super-Earth-size planet orbiting in the HZ of LHS 1140, an M4.5 dwarf at ∼15 parsecs.

Aims. In this work, we present the results of the analysis of a *Swift* X-ray/UV observing campaign. We characterize for the first time the X-ray/UV radiation environment of LHS 1140b.

Methods. We measure the variability of the near ultraviolet (NUV) flux and estimate the far ultraviolet (FUV) flux with a correlation between $FUV_{1344-1786Å}$ and $NUV_{1771-2831Å}$ flux obtained using the sample of low-mass stars in the GALEX archive. We highlight the presence of a dominating X-ray source close to the J2000 coordinates of LHS 1140, characterize its spectrum, and derive an X-ray flux upper limit for LHS 1140. We find that this contaminant source could have influenced the previously estimated spectral energy distribution.

Results. No significant variation of the $NUV_{1771-2831Å}$ flux of LHS 1140 is found over 3 months, and we do not observe any flare during the 38 ks on the target. LHS 1140 is in the 25th percentile of least variable M4-M5 dwarfs of the GALEX sample. Analyzing the UV flux experienced by the HZ planet LHS 1140b, we find that outside the atmosphere it receives a $NUV_{1771-2831Å}$ flux <2% with respect to that of the present-day Earth, while the $FUV_{1344-1786Å}/NUV_{1771-2831Å}$ ratio is ∼100–200 times higher. This represents a lower limit to the true FUV/NUV ratio since the $FUV_{1344-1786Å}$ band does not include Lyman-alpha, which dominates the FUV output of low-mass stars. This is a warning for future searches for biomarkers, which must take into account this high ratio.

Conclusions. The relatively low level and stability of UV flux experienced by LHS 1140b should be favorable for its present-day habitability.

Key words. stars: activity – planetary systems – astrobiology – stars: individual: LHS 1140

1. Introduction

In the current state of exoplanet exploration, extrasolar planets orbiting M-dwarfs represent the most promising targets to discover habitable worlds (e.g., Shields et al. 2016). Besides being the most abundant stellar population in the Galaxy (∼75%, Bochanski et al. 2010), M-dwarfs facilitate the discovery of planets with methods using transits and radial velocities (Nutzman & Charbonneau 2008; Quirrenbach et al. 2014). Moreover, given their low masses, M-dwarfs are extremely long-lived and offer long timescales for possible biological evolution on their orbiting planets (Shields et al. 2016). The habitable zone (HZ) is typically defined as the orbital distance at which the steady stellar irradiation leads to a suitable temperature for the presence of liquid water on the planetary surface (e.g., Kasting et al. 1993; Kopparapu et al. 2013). Recent exoplanet population studies suggest that planets orbiting M-dwarfs are common: in particular, Dressing & Charbonneau (2015) estimated that on average, for every seven M-dwarfs, there is at least one Earth-size planet orbiting in the HZ. The HZ of M-dwarfs is closer (∼0.1 AU) to the star with respect to earlier spectral types, and they are also

known to be very strong X-ray/UV emitters as a consequence of magnetic activity in their outer atmospheres. This implies a possible higher exposure of HZ exoplanets orbiting M-dwarfs to a variable and energetic environment. France et al. (2013) highlighted the possibility that the high-energy variability of M-dwarfs occurs with strong flare behaviors, even in M-dwarfs previously considered to be weakly active (see also Loyd et al. 2018). This high-energy environment has several implications for the evolution of the HZ planets orbiting M-dwarfs and for the possible emergence of life.

X-ray coronal emission is one of the main drivers of planetary atmospheric erosion (Sanz-Forcada et al. 2010). Ultraviolet radiation can inhibit photosynthesis, induce DNA destruction, cause damage to various species of proteins and lipids (Buccino et al. 2007), and destroy nascent biomolecules (Sagan 1973). On the other hand, as suggested by recent experimental and theoretical studies (Ranjan et al. 2017), UV radiation is a crucial element for prebiotic photochemistry, and especially for the synthesis of RNA, which favors the emergence of life. In addition, the far UV (FUV, 912–1700 Å) emission of M-dwarfs is usually comparable

with the solar one, while the near UV (NUV, 1700–3200 Å) flux of M-dwarfs seen by an exoplanet in the habitable zone can be up to three orders of magnitude fainter than the solar radiation received at Earth (France et al. 2012, 2013). This kind of emission has several implications for the atmospheric composition of planets and can lead to the formation of false-positive biosignatures (Tian et al. 2014). Indeed, as suggested by Harman et al. (2015), the typical FUV/NUV emission of M-dwarfs can induce the abiotic production of O_2 through photolysis of CO_2 followed by recombination of O atoms. This is only one of the numerous abiotic oxygen-formation pathways hypothesized in the literature. For example, abiotic O_2 can also be produced in HZ planets by the runaway greenhouse effect after planet formation due to the superluminous pre-main sequence phase of M-dwarfs (Luger & Barnes 2015), or in atmospheres with low amounts of noncondensing gases without a cold trap (Wordsworth & Pierrehumbert 2014; see also Schwieterman et al. 2018 for a recent review). For these reasons, the characterization of the emission of M-dwarfs in UV bands is crucial to constraining the possibility of life as we know it forming and surviving in their HZs. In this work we use the GALEX far UV (FUV_G, 1344–1786 Å) and the GALEX near UV (NUV_G, 1771–2831 Å) bandpasses to compare LHS 1140 with a large sample of M-dwarfs. We note that the GALEX bandpasses do not include important spectral tracers (e.g., Lyman-α, Mg II, C II, NV) and therefore only encompass part of the astrobiologically important UV irradiance band.

LHS 1140 is among the most interesting systems discovered up to now. The parent star is a M4.5 dwarf ($0.179\,M_\odot$, $0.2139\,R_\odot$) with a rotational period of ~131 days (Dittmann et al. 2017; Newton et al. 2018). It hosts LHS 1140b (Dittmann et al. 2017), a super-Earth-size planet in the HZ that transits the host star every ~24.7 days, for which both radius and mass could be measured (Dittmann et al. 2017). Recently, a further two planets were proposed to be hosted in the system, with periods of ~3.8 and ~90 days, with a more in-depth analysis of radial-velocity data (Feng et al. 2018). Independently, the shorter-period planet was also found to transit its host (Ment et al. 2019). The properties of the host star and its planets were recomputed (Kane 2018) after the new Gaia DR2 (Gaia Collaboration 2018) parallax (14.993 ± 0.015 pc). While LHS 1140b still orbits in the HZ (but with more incident flux from the star), its newly estimated radius is larger by ~20% ($1.73\,R_\oplus$) with a consequent strong reduction of the planet density and a higher suitability for transmission spectroscopy studies. The day-side equilibrium temperature estimated by Ment et al. (2019), assuming a zero Bond albedo, is 235 K which would imply that the planet is in a snowball state. However, as Del Genio et al. (2018) recall, the equilibrium temperature does not take into account the atmospheric greenhouse effect that increases the surface temperature of planets and, in the case of LHS 1140b, the chances of habitability. We note that, given the small distance from its parent star, LHS1140b is possibly tidally locked (Barnes 2017). The LHS 1140 system represents a primary target for present and future exoplanet research. In view of the above, in order to characterize the possibility of life (as we know it) emerging on the HZ planet LHS1140b, it is important to characterize its high-energy environment. We consider the high-energy FUV, NUV, and XUV (5–911 Å) radiation bands (France et al. 2016). In this work, we present the results of the analysis of a 38-ks Swift X-ray/UV observing campaign (Cycle 14; Sect. 2). We derive an upper limit on the stellar X-ray emission (Sect. 3), and characterize for the first time UV properties and variability (Sect. 4). Our results are discussed in the context of UV illumination for the exoplanet LHS 1140b.

2. Observations and data analysis

Observations of LHS 1140 were performed with the *Neil Gehrels Swift* Observatory (Gehrels et al. 2004) through a dedicated project (PI: F. Borsa). *Swift* obtains X-ray and UV data simultaneously thanks to the co-aligned XRT and UVOT. Seventeen observations, none of which were performed during planetary transits, are distributed between December 2017 and February 2018. Table 1 lists the observation log.

2.1. Swift UVOT

UVOT images (taken with the UVW2 filter) were analyzed with the public software `HEASOFT (v6.25)` package. The most recent version of the calibration database was used. All exposures within each observation were summed together. Photometry was performed within a circular source-extraction region of 5 arcsec in radius. The background was extracted from a circular region with a radius of about 20 arcsec, close to our target but without contamination from other sources. A bright UV source (Fig. 1) is detected at RA = 00 h 44 m 59.6 s and Dec = −15° 16′ 28.5′′ (Fig. 1). This position is ~12 arcsec off the J2000 coordinates of LHS 1140: this offset is consistent with the proper motion of the source[1], that is, 317.585 ± 0.121 mas yr^{-1} in right ascension and -596.617 ± 0.085 mas yr^{-1} in declination. The position of LHS 1140 in our UV image matches the one reported in the *Gaia* Archive[2]. The source was detected with a significance of between 3.3σ and 19.7σ in the 17 epochs. The magnitude and flux density of the individual epochs (as reported in Table 1) were computed with the tool `uvotsource`. We also stacked all the observations together with the tool `uvotimsum` to obtain an average flux density and produce the image shown in Fig. 1.

2.2. Swift XRT

All *Swift* XRT observations were combined in a single data set of ~38 ksec through the public service of the University of Leicester[3] and the image and spectrum accumulated over this time interval were retrieved. The analysis of the X-ray image was performed with `Ximage (v4.5.1)`. A source close to the J2000 coordinates of LHS 1140 is detected with a 3.2σ significance. This was obtained with the `sosta` tool of `Ximage` by selecting a box region with a half radius of 18.2 pixels (centered on the source). This source has a count rate of $(5.44 \pm 1.70) \times 10^{-4}$ counts s^{-1}. In Fig. 1 the X-ray contours are shown (green lines) overlayed on the UV image. The centroid of the X-ray emission does not coincide with the position (evolved at the epoch of our observations for the high proper motion) of LHS 1140 as detected in the simultaneous UVOT observations. The separation between LHS 1140 and the centroid of the X-ray emission is ~11 arcsec. However, the X-ray contours show some extension towards the present position of LHS 1140 (see Fig. 1). By searching in the PanSTARRS archive[4] we found that the possible X-ray emission centroid is coincident with a background optical source (it is unlikely to be a foreground source given the distance of our target).

We further investigated the properties of this contaminating X-ray source by exploiting our XRT observation. Data were extracted from a circular region with a radius of 20 pixels.

---

[1] http://simbad.u-strasbg.fr/simbad/sim-id?Ident=LHS+1140
[2] https://gea.esac.esa.int/archive/
[3] http://www.swift.ac.uk/user_objects/
[4] https://catalogs.mast.stsci.edu/

Table 1. UVOT observations of LHS 1140 with UVW2 filter.

Observation id	Date	Exposure time (s)	mag(AB)	Flux density (2032Å) (mJy)
87541001	2017 Nov. 08	393.18	21.65 ± 0.30	0.0079 ± 0.0022
87541002	2017 Nov. 09	757.82	21.20 ± 0.16	0.0120 ± 0.0017
87541003	2017 Nov. 11	207.83	21.31 ± 0.33	0.0109 ± 0.0033
87541004	2017 Dec. 14	317.92	21.34 ± 0.27	0.0105 ± 0.0026
87541005	2017 Dec. 22	284.56	21.08 ± 0.25	0.0135 ± 0.0031
87541006	2017 Dec. 24	2894.13	21.13 ± 0.08	0.0128 ± 0.0010
87541007	2017 Dec. 30	2316.91	21.15 ± 0.10	0.0126 ± 0.0011
87541008	2018 Jan. 03	1629.47	21.12 ± 0.11	0.0129 ± 0.0013
87541009	2018 Jan. 19	1517.95	21.12 ± 0.11	0.0130 ± 0.0014
87541010	2018 Jan. 26	6843.58	21.14 ± 0.06	0.0127 ± 0.0003
87541011	2018 Jan. 29	6869.48	21.15 ± 0.06	0.0126 ± 0.0007
87541012	2018 Jan. 31	5143.95	21.18 ± 0.07	0.0122 ± 0.0008
87541013	2018 Feb. 01	1696.71	21.02 ± 0.10	0.0142 ± 0.0014
87541014	2018 Feb. 02	1440.95	21.27 ± 0.14	0.0112 ± 0.0014
87541015	2018 Feb. 04	1096.43	21.13 ± 0.15	0.0128 ± 0.0018
87541016	2018 Feb. 06	1408.11	21.19 ± 0.14	0.0121 ± 0.0015
87541017	2018 Feb. 08	2549.22	21.01 ± 0.09	0.0143 ± 0.0012
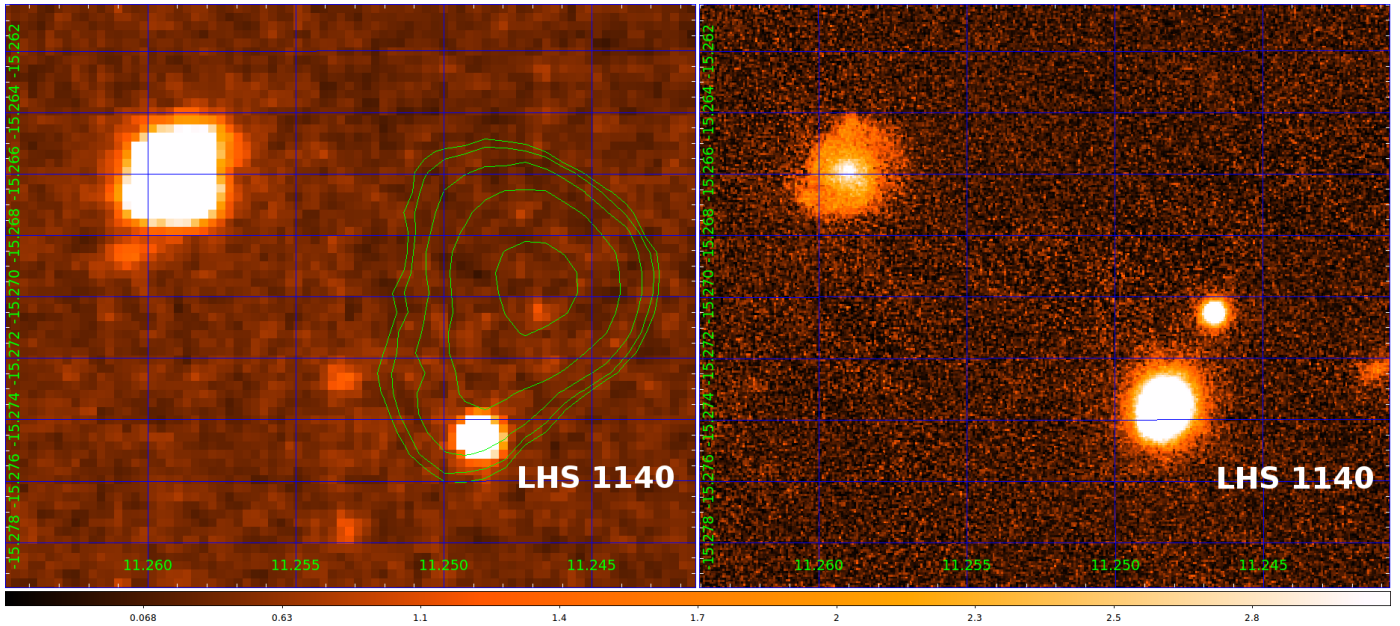
Fig. 1. *Left panel*: *Swift* UVOT UVW2 filter image (color) with overlay contour levels of the XRT image (green lines). The XRT centroid coincides with a background source present in the PanSTARRS archive. *Right panel*: PanSTARRS image (*g* band) obtained with observations between 2009 and 2014. The coordinates of LHS 1140 do not coincide in these two images due to its proper motion. The object in the upper left is LEDA 913494, a galaxy present in the Hyperleda database (Paturel et al. 2003).

Background data were extracted from a larger region close-by, devoid of sources. Source photons were then binned to have 20 counts per spectral bin. The spectrum was analyzed with the Xspec (v12.9). The low signal does not allow for a more refined characterization than a single power law (with an absorption column density fixed to the value $N_H = 5 \times 10^{18}$ cm^{-2}, in agreement with LIC model of Redfield & Linsky 2000, 2008)[5]. The power-law photon spectral index is $\Gamma = 1.78^{+1.07}_{-0.92}$ (90% confidence error interval) and the reduced $\tilde{\chi}^2 = 0.8$ (13 degrees of freedom). The unabsorbed source flux (integrated in the 0.3–10 keV energy range) is $1.42^{+0.66}_{-0.45} \times 10^{-14}$ erg cm^{-2} s^{-1}.

Given the elongated shape of the X-ray emission as observed by XRT, we estimated a 3σ upper limit on the possible X-ray flux at the position of LHS 1140 by masking the counts of the dominating source. We derive a count rate upper limit of 4.95×10^{-4} counts s^{-1} at the current position of LHS 1140. Assuming the spectrum of the contaminating X-ray source, we estimate a 3σ upper limit on the flux (integrated in the 0.3–10 keV energy range) of $\sim 1.29 \times 10^{-14}$ erg cm^{-2} s^{-1} and a flux upper limit of $\sim 3.20 \times 10^{-15}$ erg cm^{-2} s^{-1} keV^{-1} at 1 keV. We estimate an X-ray luminosity (0.1–3 keV) of $\sim 3 \times 10^{26}$ erg s^{-1} which, given the uncertainties, is consistent with typical values observed in M-dwarfs (e.g., Guinan et al. 2016; Wheatley et al. 2017).

---

[5] http://lism.wesleyan.edu/ColoradoLIC.html

3. Results

Figure 2 shows the flux-density light curve of LHS 1140 as obtained from the 17 UVOT observations (Table 1). Our UV flux observations, being centered at 2032 Å, are in the NUV_G band. No significant variations of the UV flux of LHS 1140 are found over the 17 observations distributed over almost 3 months. A Generalized Lomb Scargle analysis (Zechmeister & Kürster 2009) does not identify any significant periodicity in our UV flux light curve. Unfortunately, our time coverage (~90 d) is shorter than the rotational period (~131 d): this hampers detection of a possible rotational modulation. As an alternative method to quantify the UV variability, we used the MAD_{rel} index (Miles & Shkolnik 2017). We applied this method to LHS 1140, estimating the median absolute deviation divided by the median of the NUV_G flux. To account for the errors on the flux we generated 10^4 samples of 17 observations with a Monte Carlo sampling. The mean and standard deviation of the MAD_{rel} of these samples are 0.09 ± 0.03.

Miles & Shkolnik (2017) used simultaneous NUV_G and FUV_G observations of 145 low-mass stars taken from the sample of low-mass stars with multiple GALEX ultraviolet observations (GUV) in the GALEX archive[6] to find the correlation between NUV_G and FUV_G emission for each spectral type. The NUV and FUV GALEX data were also used by Stelzer et al. (2013) to study M-dwarfs activity. To quantify the variability of the NUV_G flux of LHS 1140 we compared its MAD_{rel} with a sample of 98 M-dwarfs (from M4 to M5 spectral type: 38 M4, 6 M4.1, 1 M4.2, 3 M4.3, 31 M4.5, 1 M4.8, 2 M4.9, 16 M5) selected from the GUV sample. Our value for LHS 1140 is the 25th percentile for the MAD_{rel} distribution of the sample. LHS 1140 is in the group of least variable M4-M5 dwarfs.

To estimate the FUV_G flux of LHS 1140 from the NUV_G flux observed by UVOT, we selected 57 M-dwarfs (of spectral type from M4 to M5) with simultaneous NUV_G and FUV_G observations from the GUV sample. From this sample, a source with an evident FUV_G flare (as noted also in Miles & Shkolnik 2017) was removed. The NUV_G and FUV_G fluxes in the GALEX archive are already scaled to a distance of 10 pc. These data are shown in Fig. 3. A least-squares fit produces the following log-correlation:
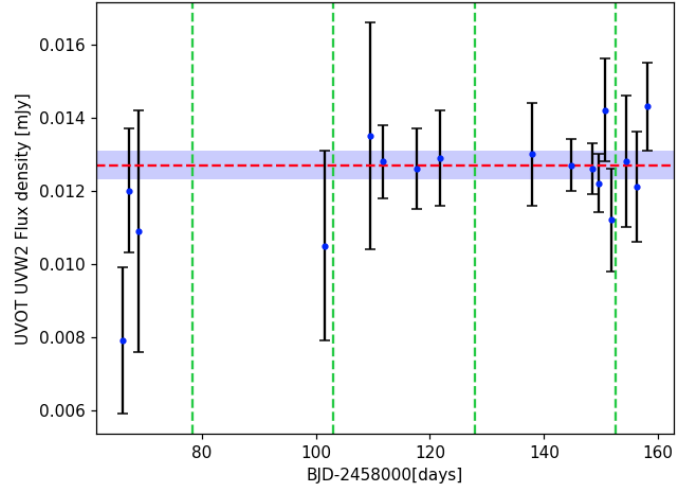
$$\mathrm{Log}(f_{FUV_G}) = 0.847(\pm 0.05) \times \mathrm{Log}(f_{NUV_G}) - 0.145(\pm 0.09). \quad (1)$$

For LHS 1140, the NUV_G flux scaled to 10 pc is $28.6 \pm 0.9\,\mu\mathrm{Jy}$. The scatter of the data points computed perpendicular with respect to the best-fit correlation was modeled with a Gaussian distribution. Using Eq. (1) we estimated for LHS 1140 a FUV_G flux scaled to 10 pc of $12.2 \pm 2.4\,\mu\mathrm{Jy}$. We measure a NUV magnitude (AB system) of 21.1, while our estimated FUV magnitude is 22.1. These values are consistent with the nondetection of our target in the GALEX AIS (All Sky Imaging Survey) images. In fact, the GALEX AIS data reach limit magnitudes (5σ) of 20.8 for the NUV and 19.9 for the FUV (Morrissey et al. 2007).

In addition, in Sect. 2.2 we report the discovery of a contaminating X-ray source that was close to LHS 1140 around the year 2000 but is no longer found in such proximity thanks to the high proper motion of LHS 1140. We therefore visually inspected the images available in the literature[7] and reported in Table 2, to check if the two sources (LHS 1140 and the contaminant one) were superposed. In the end we decided to exclude the

[6] http://vizier.cfa.harvard.edu/viz-bin/VizieR?-source=J/AJ/154/67
[7] From CDS Portal https://cds.u-strasbg.fr/

Fig. 2. LHS 1140 UVOT-UVW2 flux-density light curve. Error bars represent the 1σ uncertainty. The vertical green dashed lines are the epochs of transit of LHS 1140b. The horizontal dashed red line is the average flux density ($12.7\,\mu\mathrm{Jy}$) as obtained from the analysis of the stacked UV image (Fig. 1) with its 1σ uncertainty ($0.4\,\mu\mathrm{Jy}$, shaded region).
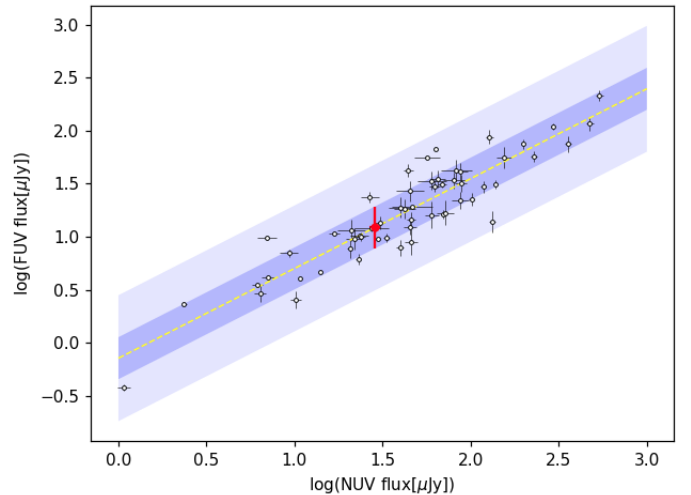
Fig. 3. Correlation between the FUV_G and the NUV_G flux density of M4-M5 stars. The yellow dashed line is the least-squares fit of the data points. The red point shows the position of LHS 1140 as obtained through our measure of the NUV_G flux density (Sect. 2). The shaded regions mark the 1σ and 3σ dispersion (measured perpendicular to the best fit line) of the data points.

2MASS data, which were collected between 1997 June and 2001 February because in the corresponding images LHS 1140 and the background source were spatially coincident. Figure 4 shows a plot of the spectral energy distribution (SED) of the star and the black-body temperature recalculated using only fluxes obtained from optical and IR images where the two sources are resolved. We did not use the UV fluxes because of the known chromospheric M-dwarfs emission (e.g., France et al. 2013; Stelzer et al. 2016). We obtain a new estimate of effective temperature of LHS 1140 $T_{eff} = 3016 \pm 29$ K, which is ~200 K lower than previous estimates.

4. Discussion and conclusions

We measure a NUV_G luminosity for LHS 1140 of $(2.63 \pm 0.09) \times 10^{27}$ erg s^{-1}, and estimate the FUV_G luminosity to be $(7.97 \pm 1.57) \times 10^{26}$ erg s^{-1}. We subsequently attempted to

Table 2. Optical and IR LHS1140 flux measurements used in Fig. 4.

Filter	Flux (Jy)	Flux err (Jy)
Gaia:G	0.0318	0.0001
Gaia/*Gaia*2:Grp	0.0722	0.0001
Gaia/*Gaia*2:G	0.0282	0.0001
Gaia/*Gaia*2:Gbp	0.00595	0.00002
WISE:W4	0.0046	0.0011
WISE:W3	0.0147	0.0003
WISE:W2	0.0751	0.0013
WISE:W1	0.111	0.002
PAN-STARRS/PS1:g	0.00459	0.00002
2MASS:Ks	0.2	0.004
2MASS:H	0.242	0.006
2MASS:J	0.225	0.005

Notes. CDS Portal (`http://cdsportal.u-strasbg.fr/?target=lhs1140`) in the Photometric Points section. Due to suspicion of possible contamination, we did not use 2MASS data for the effective temperature fit.
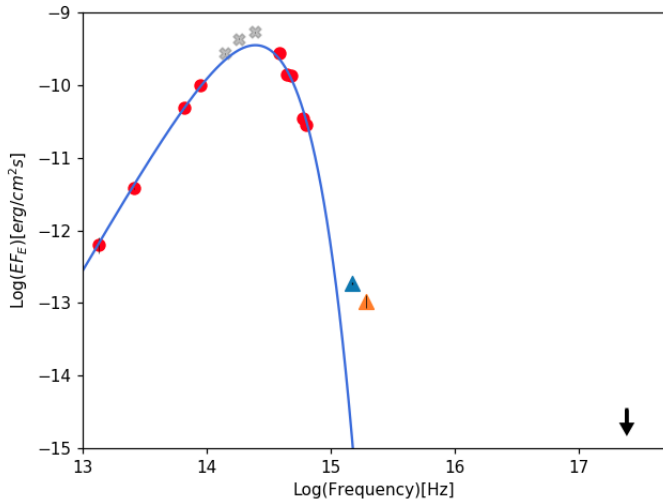
Fig. 4. LHS 1140 EF_E SED, calculated with data from the CDS. The points are listed in Table 2. Red points mark the black-body temperature estimation. Gray symbols are 2MASS data. UVOT UVW2 NUV flux is represented by the blue triangle. FUV_G flux estimated with $FUV_G - NUV_G$ correlation is represented by the orange triangle. The black arrow shows the 3σ upper limit to the X-ray flux of LHS 1140 at 1 keV. The blue line is the black body model with a temperature of 3015 K.

elucidate the FUV/NUV environment reaching the HZ planet LHS 1140b in the context of that of the present-day Earth. We refer to fluxes arriving outside the atmospheres, not taking into account possible atmospheric differences between Earth and LHS 1140b. Future atmospheric investigations of LHS 1140b will allow us to also put constraints on the UV environment on the planetary surface.

We estimated the present-day Earth UV flux by calculating the integrated flux of the quiet Sun in its HZ (Woods et al. 2009; France et al. 2012) in our NUV_G and FUV_G bands ($NUV_\oplus$, $FUV_\oplus$). We find $NUV_\oplus = 6.4 \times 10^3$ erg cm^{-2} s^{-1} and $FUV_\oplus = 11.8$ erg cm^{-2} s^{-1}. To measure the NUV_G and the FUV_G integrated flux on LHS 1140b (NUV_{LHS}, FUV_{LHS}), we scaled the flux observed with *Swift* at the semi-major axis distance from LHS 1140 (0.0936AU, Ment et al. 2019) assuming that the fluxes are constant in each band. We find $NUV_{LHS} = 106.8 \pm 6.2$ erg cm^{-2} s^{-1} (0.017 ± 0.001 $NUV_\oplus$) and

$FUV_{LHS} = 32.4 \pm 7.2$ erg cm^{-2} s^{-1} (2.75 ± 0.61 $FUV_\oplus$). The FUV_G/NUV_G integrated flux ratio reaching LHS 1140b is $\sim$100–200 times greater than the ratio reaching Earth at present. Since the GALEX UV bandpasses do not include Lyman-alpha, which dominates the FUV output of low-mass stars, this represents a lower limit to the true top-of-atmosphere FUV/NUV ratio.

Both FUV and NUV illumination are relevant for oxygen photochemistry. For example, FUV photons dissociating CO_2 can be net sources of abiotic atmospheric oxygen (Tian et al. 2014). Therefore, in an atmosphere with a high concentration of CO_2 and a high FUV/NUV ratio, detection of oxygen in combination with H_2O does not necessarily imply the existence of life, contrary to what was previously thought. This high FUV/NUV ratio could therefore lead to the formation of possible false-positive biosignatures: this is a warning for future atmospheric observations of LHS 1140b. As mentioned in the introduction to this paper, the photolysis of CO_2 is only one of the numerous abiotic oxygen-formation pathways.

The low level of NUV flux seen by LHS 1140b could be negative for abiogenesis (Ranjan et al. 2017). This result is consistent with Rimmer et al. (2018), who place LHS 1140b out of the abiogenesis zone. In this context it is still not clear if the UV-dependent prebiotic pathways that were important for the origin of life on Earth can still proceed in a lower UV environment (Ranjan et al. 2017) such as that of LHS 1140b. In any case, the activity evolution of M-dwarfs, even though still not completely understood, seems to decrease with age (Ribas et al. 2016; Claire et al. 2012; Selsis et al. 2007; Guinan et al. 2016) implying that LHS 1140b could have suffered more high-energy irradiance in the past. Flares could also provide the missing UV energy for abiogenesis (Buccino et al. 2007), though we do not observe flares during our observations, possibly favoring current habitability. However, we cannot exclude that flares occur in a time-span that is different from our observations or that flare activity was present in the past.

Since the relative distances between planets orbiting M-dwarfs are usually smaller than between planets around other stellar types, the probability of a panspermia scenario could increase (Lingam & Loeb 2017). Life could emerge on a planet with enough NUV irradiation, and eventually migrate to an outer planet where the flux of potentially destructive high-energy photons is not critical. Therefore, we estimated the NUV_G flux experienced by LHS 1140c (semi-major axis: 0.02675 ± 0.00070 AU, Ment et al. 2019): 1308 ± 43 erg cm^{-2} s^{-1}, approximately 12 times greater than the NUV_G flux seen by LHS 1140b and 4.9 times lower than that seen by present-day Earth.

In view of the many studies of M-dwarfs considering UV radiation as deleterious for life (e.g., Setlow 1974; Heath et al. 1999; Tarter et al. 2007; Lammer et al. 2009; Shields et al. 2016; Meadows et al. 2017) and of the UV luminosity of LHS 1140 that we measured with *Swift* observations, the relatively low level and stability of UV flux experienced by LHS 1140b should be favorable for its present-day habitability.

References

Barnes, R. 2017, Celest. Mech. Dyn. Astron., 129, 509
Benedict, G. F., Henry, T. J., Franz, O. G., et al. 2016, AJ, 152, 141
Bochanski, J. J., Hawley, S. L., Covey, K. R., et al. 2010, AJ, 139, 2679
Buccino, A. P., Lemarchand, G. A., & Mauas, P. J. D. 2007, Icarus, 192, 582
Claire, M. W., Sheets, J., Cohen, M., et al. 2012, ApJ, 757, 95
Del Genio, A. D., Kiang, N. Y., Way, M. J., et al. 2018, ApJ, submitted [arXiv:1812.06606]
Dittmann, J. A., Irwin, J. M., Charbonneau, D., et al. 2017, Nature, 544, 333
Dressing, C. D., & Charbonneau, D. 2015, ApJ, 807, 45
Feng, F., Tuomi, M., & Jones, H. R. A. 2018, MNRAS, submitted [arXiv:1807.02483]
France, K., Linsky, J. L., Tian, F., Froning, C. S., & Roberge, A. 2012, ApJ, 750, L32
France, K., Froning, C. S., Linsky, J. L., et al. 2013, ApJ, 763, 149
France, K., Loyd, R. O. P., Youngblood, A., et al. 2016, ApJ, 820, 89
Gaia Collaboration (Brown, A. G. A., et al.) 2018, A&A, 616, A1
Gehrels, N., Chincarini, G., Giommi, P., et al. 2004, ApJ, 611, 1005
Guinan, E. F., Engle, S. G., & Durbin, A. 2016, ApJ, 821, 81
Harman, C. E., Schwieterman, E. W., Schottelkotte, J. C., & Kasting, J. F. 2015, ApJ, 812, 137
Heath, M. J., Doyle, L. R., Joshi, M. M., & Haberle, R. M. 1999, Orig. Life Evol. Biosph., 29, 405
Kane, S. R. 2018, ApJ, 861, L21
Kasting, J. F., Whitmire, D. P., & Reynolds, R. T. 1993, Icarus, 101, 108
Kopparapu, R. K., Ramirez, R., Kasting, J. F., et al. 2013, ApJ, 765, 131
Lammer, H., Bredehöft, J. H., Coustenis, A., et al. 2009, A&ARv, 17, 181
Lingam, M., & Loeb, A. 2017, Proc. Natl. Acad. Sci., 114, 6689
Linsky, J. 2014, Challenges, 5, 351
Loyd, R. O. P., France, K., Youngblood, A., et al. 2018, ApJ, 867, 71
Luger, R., & Barnes, R. 2015, Astrobiology, 15, 119
Meadows, V., Arney, G., Schwieterman, E., et al. 2017, AAS Meeting Abstracts, 229, 120.03
Ment, K., Dittmann, J. A., Astudillo-Defru, N., et al. 2019, AJ, 157, 32
Miles, B. E., & Shkolnik, E. L. 2017, AJ, 154, 67
Morrissey, P., Conrow, T., Barlow, T. A., et al. 2007, ApJS, 173, 682
Newton, E. R., Mondrik, N., Irwin, J., Winters, J. G., & Charbonneau, D. 2018, AJ, 156, 217
Nutzman, P., & Charbonneau, D. 2008, PASP, 120, 317
Paturel, G., Petit, C., Prugniel, P., et al. 2003, A&A, 412, 45
Quirrenbach, A., Amado, P. J., Caballero, J. A., et al. 2014, Exploring the Formation and Evolution of Planetary Systems (Cambridge: Cambridge University Press), 299, 395
Ranjan, S., Wordsworth, R., & Sasselov, D. D. 2017, ApJ, 843, 110
Redfield, S., & Linsky, J. L. 2000, ApJ, 534, 825
Redfield, S., & Linsky, J. L. 2008, ApJ, 673, 283
Ribas, I., Bolmont, E., Selsis, F., et al. 2016, A&A, 596, A111
Rimmer, P. B., Xu, J., Thompson, S. J., et al. 2018, Sci. Adv., 4, 3302
Sagan, C. 1973, J. Theor. Biol., 39, 195
Sanz-Forcada, J., Ribas, I., Micela, G., et al. 2010, A&A, 511, L8
Schneider, A. C., & Shkolnik, E. L. 2018, AJ, 155, 122
Schwieterman, E. W., Kiang, N. Y., Parenteau, M. N., et al. 2018, Astrobiology, 18, 663
Selsis, F., Kasting, J. F., Levrard, B., et al. 2007, A&A, 476, 1373
Setlow, R. B. 1974, Proc. Natl. Acad. Sci., 71, 3363
Shields, A. L., Ballard, S., & Johnson, J. A. 2016, Phys. Rep., 663, 1
Stelzer, B., Marino, A., Micela, G., López-Santiago, J., & Liefke, C. 2013, MNRAS, 431, 2063
Stelzer, B., Damasso, M., Scholz, A., & Matt, S. P. 2016, MNRAS, 463, 1844
Tarter, J. C., Backus, P. R., Mancinelli, R. L., et al. 2007, Astrobiology, 7, 30
Tian, F., France, K., Linsky, J. L., Mauas, P. J. D., & Vieytes, M. C. 2014, Earth Planet. Sci. Lett., 385, 22
Wheatley, P. J., Louden, T., Bourrier, V., Ehrenreich, D., & Gillon, M. 2017, MNRAS, 465, L74
Winters, J. G., Sevrinsky, R. A., Jao, W.-C., et al. 2017, VizieR Online Data Catalog: 515
Woods, T. N., Chamberlin, P. C., Harder, J. W., et al. 2009, Geophys. Res. Lett., 36, L01101
Wordsworth, R., & Pierrehumbert, R. 2014, ApJ, 785, L20
Zechmeister, M., & Kürster, M. 2009, A&A, 496, 577